Hyperspectral image fusion by multiplication of spectral constraint and NMF

Zhenyu An, Zhenwei Shi *

Image Processing Center, School of Astronautics, Beijing University of Aeronautics and Astronautics, Beijing 100191, P.R. China

Abstract

Hyperspectral remote sensing has been used in many fields, such as agriculture, military detection and mineral exploration. Hyperspectral image (HSI), despite its high spectral resolution, has lower spatial resolution than panchromatic image (PI). Therefore, it is useful yet still challenging to effectively fuse HSI and PI to obtain images with both high spectral resolution and high spatial resolution. To solve the problem, a new HSI fusion method based on multiplication of spectral constraint and non-negative matrix factorization is proposed in the paper. In the model, the HSI is first decomposed into basis (abundance matrix) and weight (spectral matrix), then the details of HSI are sharpened by enhancing the details of the abundance with PI. Meanwhile, a spectral constraint term is proposed. It is used to specifically preserve the spectral information in the model. Therefore, the fused data is characterized by good spatial and spectral information. Finally, experiments with both simulated and real data are implemented and the results show that the proposed method performs better in both visual analysis and objective indices than conventional methods, thus making it a good choice for HSI fusion.

Key words: Hyperspectral Image Fusion; Non-negative Matrix Factorization; Spectral Constraint; Quality Analysis

* Corresponding author. Tel.: +86-10-823-39-520; Fax: +86-10-823-38-798. The work was supported by the National Natural Science Foundation of China under the Grants 61273245 and 91120301, the 973 Program under the Grant 2010CB327904, the open funding project of State Key Laboratory of Virtual Reality Technology and Systems, Beihang University (Grant No. BUAA-VR-12KF-07), and Program for New Century Excellent Talents in University of Ministry of Education of China under the Grant NCET-11-0775. The work was also supported by Beijing Key Laboratory of Digital Media, Beihang University, Beijing 100191, P.R. China.

Email address: shizhenwei@buaa.edu.cn (Zhenwei Shi).

1 Introduction

Hyperspectral remote sensing is a new remote sensing technique. Hyperspectral data, characterized by its combination of high spectral resolution and two-dimensional spatial image [16,24,44], has attracted many people's interests recently. The data contains continuous spectral curves which describe the reflectivity of different specific objects on the ground, making it play an important role in the image detection, classification, and recognition. However, due to the constraint of sensors, HSI usually has low spatial resolution, which limits its application in some circumstances. Meanwhile, panchromatic image (PI), another kind of image, can be more easily obtained with high spatial quality but insufficient spectral information. Naturally, to fuse the two different kinds of former images and obtain a new image with both ideal spatial and spectral information is a critical and useful task. Therefore, the fusion process has become a critical preprocessing step in the applications of remote sensing [31,32,34].

Various methods proposed for image fusion could be sorted into several basic categories: arithmetic methods, projection-substitution-based methods, ARSIS (the French acronym for "Amélioration de la Résolution Spatiale par Injection de Structures") concept fusion methods, model-based methods, and hybrid methods. Among these methods, the simplest way is the arithmetic methods, which are usually based on the addition or/and multiplication between the original HSI and PI. These methods cost relatively less computational time. However, the fused data usually has serious spectral distortion [8]. Projection-substitution-based methods are the popular and classic methods. In these methods, researchers transform the HSI into some other new spaces, replace one of the newly obtained components with the PI. Then, the fused data is obtained after inverse transformation. To a great extent, the quality of the fused results via these methods lies on the proper transformed space chosen, also the spectral information of the fused data usually distort in some degree. Intensity hue saturation (IHS) [10,42,43], principal component analysis (PCA) [38], Gram-Schmidt (GS) [23] transform are all the typical used methods. For methods based on the ARSIS concept, researchers assume that the high frequency components of HSIs could be obtained from those in PIs. Thus in these methods, the high-frequency information is extracted from the PIs before being injected into the HSIs. The multiresolution analyses, such as Laplacian pyramid [33], discrete wavelet transform (DWT) [22,37], and "á trous" wavelet transform (ATWT) [30,35], have been used to accomplish the fusion task. An ATWT-based method named the additive wavelet intensity method (AWLP) [3], is also a typical one. However, although they are also widely applied in image fusion, they are better suited to cases where the resolution ratio between the HSI and PI is two [47]. Model-based methods are usually based on image formulation models and some strong theoretical frame-

works. Researchers treat the fusion process as different inverse optimization problems and establish proper fusion models, respectively. Projection onto convex sets (POCS) [1], maximum a posteriori (MAP) method [17,15], variational fusion methods [2,40], non-negative matrix factorization based methods [48–51], are the representative methods. Hybrid methods, like the Ehlers method [14] (combination of the IHS method and the ARSIS method) and [27] synthesize the virtues of different fusion methods.

However, the methods mentioned above have some limitations for the fusion of HSI and PI. Most fusion methods, like PCA, wavelet transformation and IHS method, address the fusion between the multiscale image (MSI) and PI. Compared with the MSI, HSI has its special properties for its more precise spectral information. Therefore, two principles should be taken into consideration in the HSI fusion process [40]. One is the effective combination of the spatial information in two different source images, which requires the textures and details of the original images (specifically PI) being preserved in the fused data. Another is the preservation of spectral information, which means that the spectral information of the fused data should be close to that of the original hyperspectral data. Here, the spectral information means spectral slope index (SSI), spectral absorption index (SAI), and other different information that spectra contain. As in conventional methods, only several bands have been taken into consideration, the fused data will not be ideal in spatial and spectral quality simultaneity if the above methods are directly used. Thus, some researchers focus on other possible approaches. MAP methods [17,15] and variational method [40] are designed for HSI fusion, the former methods are proposed with the assumption that the fused hyperpixels are conditionally independent and the latter have complex choice of parameters. Naoto Yokoya et al., proposed to fuse HSI and MSI by using unmixing model with coupled non-negative matrix factorization [48].

Inspired by the previous work, for the fusion of HSI and PI, we propose a Multiplication of Spectral constraint and Non-negative Matrix Factorization (MS-NMF) model. In the model, HSI is first factorized into basis (abundance matrix) and weight (endmember matrix) with the MS-NMF, then the abundance matrix is sharpened with the PI. Finally, the HSI is reconstructed with the constraint of spectral preservation. Note that, since the abundance matrix has been sharpened, the fusion process is completed with the reconstruction process. Meanwhile, the spectral information is also exploited in the model, thus making the fused data preserve the information of original spectra. We will see that the proposed method has the following main advantages: Direct constraint on the spectra of HSI; Effectively enhancement on the details; Wide extendibility for more in-depth research.

The rest of paper is organized as follows: In Section 2, conventional NMF and its application in HSI is introduced. In section 3, we establish the MS-

NMF model to deal with the HSI fusion problem, then use the steepest descent method to solve the extremal function. Finally, we evaluate our method by the simulated and real data experiments in Section 4, and followed by conclusions in Section 5.

2 Non-negative Matrix Factorization (NMF)

Given a non-negative matrix $\mathbf{V}$, NMF finds two non-negative matrices $\mathbf{W}$ and $\mathbf{H}$ to satisfy:

$$\mathbf{V} \approx \mathbf{WH} \tag{1}$$

The matrix $\mathbf{V} \in \mathbb{R}^{N\times K}$ is approximately factorized into the multiplication of $\mathbf{W} \in \mathbb{R}^{N\times L}$ and $\mathbf{H} \in \mathbb{R}^{L\times K}$. $\mathbf{W}$ is a basis which is optimized for linear approximation of the data set $\mathbf{V}$, $\mathbf{H}$ is the coefficient matrix of the data set $\mathbf{V}$ projected on basis of $\mathbf{W}$ [26].

To find out an approximate factorization result satisfying $\mathbf{V} \approx \mathbf{WH}$ for NMF, an objective function should be defined. It is able to quantify the quality of the approximation. One useful measurement is the square of the Euclidean distance [11] between $\mathbf{V}$ and $\mathbf{WH}$:

$$F(\mathbf{W},\mathbf{H}) = \frac{1}{2}\sum_i\sum_j \left(\mathbf{V}_{ij} - (\mathbf{WH})_{ij}\right)^2 = \frac{1}{2}\left\|\mathbf{V}-\mathbf{WH}\right\|^2 \tag{2}$$

Lee and Seung [26] used a multiplicative update rule for minimizing the object function as follows:

$$\mathbf{W} \leftarrow \mathbf{W}.*(\mathbf{VH}^T)./(\mathbf{WHH}^T+\varepsilon) \tag{3}$$
$$\mathbf{H} \leftarrow \mathbf{H}.*(\mathbf{W}^T\mathbf{V})./(\mathbf{W}^T\mathbf{WH}+\varepsilon) \tag{4}$$

where $.*$ and $./$ denote elementwise multiplication and division, respectively. ε is an extremely small non-negative number in computing for insuring the denominator non-zero. Therefore, so long as the initialization is non-negative, the rule insures matrices non-negative.

Use it to decompose the hyperspectral data $\mathbf{V} \in \mathbb{R}^{N\times K}$ with K bands and N pixels, then the results $\mathbf{W}$ and $\mathbf{H}$ are obtained as illustrated in Fig. 1. Note that before the factorization, image of each band is scattered to a column vector. The result $\mathbf{W} = [\mathbf{W}_1, ..., \mathbf{W}_L] \in \mathbb{R}^{N\times L}$ $(L \leq K)$ is the matrix of objects distribution (also named abundance matrix), and each column $\mathbf{W}_l \in \mathbb{R}^N (l \in 1, 2, ..., L)$ corresponds to a pure object on the ground. $\mathbf{H} \in \mathbb{R}^{L\times K}$ (also named endmember matrix) represents the spectral reflection of the objects like tree,

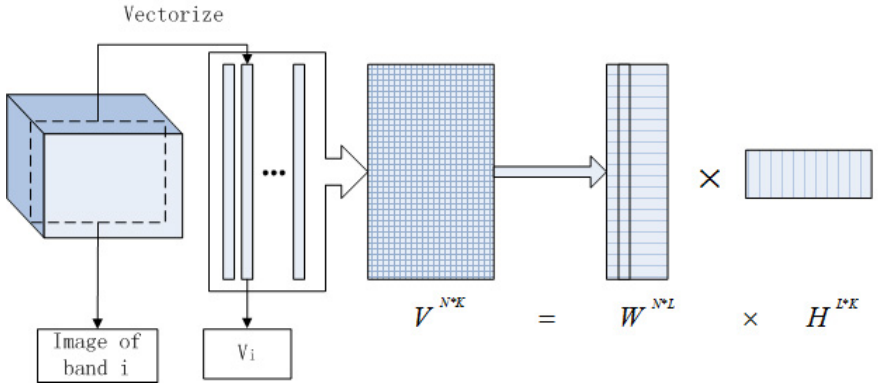

Fig. 1. The decomposition on the HSI data via NMF.

river and roof. L is the number of pure objects in the scene. Therefore, we reconstruct the hyperspectral data $\mathbf{V}$ by $\mathbf{V} \approx \mathbf{W} * \mathbf{H}$, where $\mathbf{W}$ and $\mathbf{H}$ are the previously decomposed results.

Besides the factorization form in equation (1), Karoui et al. proposed another form in [20]. In their method, image of each band is scattered to a row vector before the factorization. Therefore, the factorization form becomes:

$$\mathbf{V}^{K\times N} \approx \mathbf{H}^{K\times L}\mathbf{W}^{L\times N} \tag{5}$$

where K, N, and L represent the band number, pixel number and pure object number, respectively. $\mathbf{W}$ and $\mathbf{H}$ represent the abundance matrix and endmember matrix. Obviously, this form is the transposition of equation (1), and they are essentially the same mathematically. However, in equation (5), the "request for many samples is usually met" [20], and it is designed for MSI with few spectral bands, while the form in equation (1) requires "many" bands. Therefore, in the proposed fusion for HSI and PI, the form in equation (1) is adopted for the quantity of bands in HSI. In fact, NMF with form in equation (1) has been widely used in hyperspectral image processing, like unmixing [19] and feature extraction [25].

As discussed before, $\mathbf{W}$ represents the distribution of the data, so if it is enhanced with PI effectively, then the details of the reconstructed matrix $\mathbf{V}$ is sharpened. Based on the idea, MS-NMF is proposed and details are shown in the following sections.

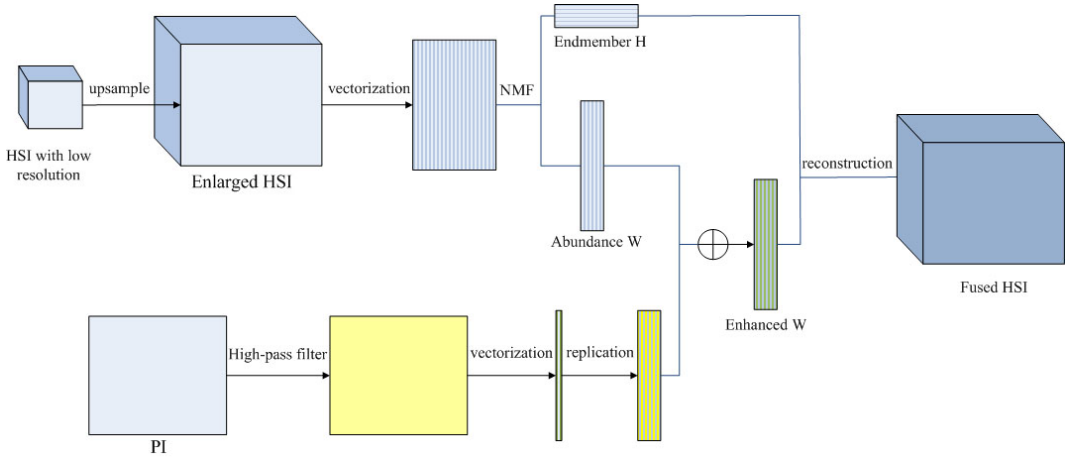

Fig. 2. Proposed fusion process via MS-NMF.

3 Hyperspectral image fusion via MS-NMF

3.1 Proposed Fusion Model

The process of MS-NMF is proposed as shown in Fig. 2. First, image of each band in the 3-D HSI is interpolated to the same spatial resolution of PI (this step is usually accomplished with the registration process). Also, the interpolated HSI is denoted as our "original HSI" in the following discussion. Scatter the interpolation data into a matrix and factorize it with NMF, then we obtain abundance matrix **W** and endmember matrix **H**. Meanwhile, using high-pass filter, we obtain the high-frequency information of PI. Then the abundance matrix **W** is enhanced with the high-frequency information. Finally, the fusion process is accomplished by the NMF reconstruction with the enhanced **W** and the endmember matrix **H**. Clearly, effective enhancement of **W**, which will be detailedly discussed in the following section, is one of the critical procedures for the fusion process.

*3.2 Enhancement of **W***

Different approaches, like addition, multiplication and division, are available for the enhancement of **W**. In our approach, we accomplish the procedure with assumption that the missing high-frequency information of the fused HSI can be extracted from the PI. The assumption is reasonable for PI is obtained with covering a broad range of the wavelength spectrum [41]. Meanwhile, as discussed before, if each column of abundance matrix **W** is transformed into a map with size of the original PI, then the obtained map represents the distribution of a particular object. Therefore, **W** could represent the scene

in HSI with reduced dimensions (only few pure endmembers, whereas much more bands in original HSI). Moreover, the abundance map has the similar spatial resolution as that of the original HSI, thus justifying the great similarity between the $\mathbf{W}$ and original HSI. Note that the assumption is also similar to those of the improved additive wavelet method of Kim et al. [21] and general image-fusion (GIF) method of Wang et al. [47]. However, it is also worth mentioning that, in view of Thomas et al. [41], object occultation and moving objects also result in some local dissimilarities, where the assumption is not fully satisfied. Therefore, in our approach, instead of the original PI, high-frequency information of PI is first extracted and then injected into the HSI. The operation could avoid the influence of the local dissimilarities caused by the object occultation to some extent yet not effective for the moving objects, thus leading the "ghost scene" in the fused data. Therefore, handling the images with moving objects remains a challenging problem for most of the fusion methods including ours. In this paper, images without moving objects are used to evaluate the fusion methods.

Based on the assumption, we first obtain the high-frequency information by filtering the original PI with a high-pass filter. Also, we could obtain the high-frequency information by subtracting the PI with low spatial resolution, which is the low-pass filtered PI. In our approach as shown in Fig. 2, high-pass filtering is used. Therefore, we have the high-frequency information denoted PI_h:

$$\mathrm{PI}_h = \mathrm{PI} * h_0 \tag{6}$$

where h_0 is a high-pass filter and * denote convolutional operation. The size of filter coincides with the resolution ratio of PI and HSI. 3×3 and 5×5 are suitable for the 1:2 and 1:4 ratio of spatial resolution between PI and HSI, respectively. After obtaining the expected high-frequency information PI_h, we then scatter it into a column vector. Replicate it into a matrix with the same column number as the $\mathbf{W}$, thus obtaining P_h with the same size of $\mathbf{W}$.

As discussed before, different methods could be applied to enhance the $\mathbf{W}$. Here, based on the assumption that the high frequency of fused HSI could be injected from the PI, we use the mean of $\mathbf{W}$ and P_h. Before the addition, P_h is normalized within the value 0 and 1 in order to regularize the different units of P_h and $\mathbf{W}$. Therefore, the approach is similar to the HPF fusion method [47], and the fusion model is obtained as follows:

$$\begin{aligned} min \quad & \mathbf{F}(\mathbf{W},\mathbf{H}) = \frac{1}{2}\left\|\mathbf{V}-\mathbf{W}\mathbf{H}\right\|^2 \\ s.t. \quad & \mathbf{W} \geq 0, \mathbf{H} \geq 0. \end{aligned} \tag{7}$$

and the fused data $\mathbf{V}_f$ is easily obtained:

$$\mathbf{V}_f = (\mathbf{W} + \mathbf{P}_h)/2 \times \mathbf{H} \tag{8}$$

Note that the enhancement is not limited to the proposed process, other more effective approaches maybe available, implying the wide extendibility of the proposed fusion model.

3.3 Constraint of spectral information

The above simple fusion process is equivalent to adding the high-frequency component $\mathbf{P}_h$ to the original HSI. This simple addition operation does not distinguish the information that the PI brought. Therefore, information redundancy usually happens for the fused HSI. Moreover, components with low frequency of PI are also brought in, resulting in the distortion of spectral information. Therefore, it remains a challenge to accomplish the fusion process while preserving the spectral signature.

Obviously, to fuse the images without changing the spectral signature at all is impossible. However, we could relax the constraint, and keep the spectral vectors as parallel as possible. Specifically, the index spectral angle mapper (SAM) is a proper choice to describe the parallelism with its definition as follows:

$$\text{SAM} = \arccos\left(\frac{\langle \vec{a}, \vec{b} \rangle}{\|\vec{a}\| \|\vec{b}\|}\right) \tag{9}$$

where $\vec{a}, \vec{b}$ respectively represent the same pixel's spectral vectors of the original and fused HSI. $\langle\rangle$ is the inner product and $\|\|$ is the Euclidian l_2-norm. Obviously, in fusion process, SAM of a pixel is expected to be zero, because the two vectors could only be parallel in this condition. Therefore, in the paper, a spectral constraint function based on SAM will be introduced to preserve the spectral signature.

Suppose $\mathbf{V}_f$ is the fused data, where $\mathbf{V}_f \in R^{N \times K}$ contains K bands, and N is the pixel number, then we have $\text{SAM} = \arccos(\frac{\langle \mathbf{V}_f(i,:), \mathbf{V}(i,:) \rangle}{\|(\mathbf{V}_f(i,:)\| \|\mathbf{V}(i,:)\|})$ for each pixel, where $\mathbf{V}_f(i,:)$ and $\mathbf{V}(i,:)$ represents the spectral vector of pixel i before and after fusion. Both of them have the size $1 \times K$. So the spectral constraint function is the summation of all the pixels:

$$\text{SAM} = \sum_{i=1}^{N} \arccos\left(\frac{\langle \mathbf{V}_f(i,:), \mathbf{V}(i,:) \rangle}{\|(\mathbf{V}_f(i,:)\| \|\mathbf{V}(i,:)\|}\right) \tag{10}$$

However, the original definition of SAM is difficult for us to establish con-

straint function, so we simplify it by using the value of its cosine instead. Therefore, we have the following term:

$$\text{SAM\_cos} = \sum_{i=1}^{N} \frac{\langle \mathbf{V}_f(i,:), \mathbf{V}(i,:) \rangle}{\|(\mathbf{V}_f(i,:)\| \|\mathbf{V}(i,:)\|} \tag{11}$$

In this form, the calculation of inverse cosine in equation (10) is avoided. However, the term SAM_cos is expected to be N instead of 0, because for each pixel i, the reference value of $\frac{\langle \mathbf{V}_f(i,:), \mathbf{V}(i,:) \rangle}{\|(\mathbf{V}_f(i,:)\| \|\mathbf{V}(i,:)\|}$ is 1. Therefore, a more available form for fusion is needed. Note that the l_2-norm in term (11) is inconvenient for the latter calculation of gradient, a quadratic form is used and we have:

$$\text{SAM\_cos\_qua} = \sum_{i=1}^{N} \frac{(\langle \mathbf{V}_f(i,:), \mathbf{V}(i,:) \rangle)^2}{(\|(\mathbf{V}_f(i,:)\| \|\mathbf{V}(i,:)\|)^2} \tag{12}$$

In the form, term SAM_cos_qua is not completely the same as SAM_cos for the quadratic operation on each pixel though both them have the reference value N. On the other hand, we have the following inequality for each pixel i. :

$$0 \leq \frac{(\langle \mathbf{V}_f(i,:), \mathbf{V}(i,:) \rangle)^2}{(\|(\mathbf{V}_f(i,:)\| \|\mathbf{V}(i,:)\|)^2} \leq 1 \tag{13}$$

Multiplying $(\|(\mathbf{V}_f(i,:)\| \|\mathbf{V}(i,:)\|)^2$ on the term, then we have

$$0 \leq (\langle \mathbf{V}_f(i,:), \mathbf{V}(i,:) \rangle)^2 \leq (\|(\mathbf{V}_f(i,:)\| \|\mathbf{V}(i,:)\|)^2 \tag{14}$$

The left half of the inequality (14) holds for the data in HSI is non-negative and the right half of inequality holds because of the original definition of vector norm. Moreover, in HSI fusion, the vector of fused data $\mathbf{V}_f(i,:)$ and the original data $\mathbf{V}(i,:)$ are expected to be parallel, thus making the term $(\|(\mathbf{V}_f(i,:)\| \times \|\mathbf{V}(i,:)\|)^2 - (\langle \mathbf{V}_f(i,:), \mathbf{V}(i,:) \rangle)^2$ close to 0. Therefore, to establish the spectral constraint function, we use this form and obtain the following term:

$$\mathbf{S}(\mathbf{V}_{f(\mathbf{W},\mathbf{H})}) = \sum_{i=1}^{N} (\|(\mathbf{V}_f(i,:)\|^2 \|\mathbf{V}(i,:)\|^2 - (\langle \mathbf{V}_f(i,:), \mathbf{V}(i,:) \rangle)^2) \tag{15}$$

Note that the form of term (15) seems to be quite different from the original definition of SAM. However, it could represent the parallel degree between the

fused HSI and the original HSI with reference value 0. Moreover, the closer to 0, the spectral information in fused HSI and original HSI are more identical. Therefore, term (15) will be applied to preserve the spectral information in HSI fusion. On the other hand, term (15) is still not convenient because of the vector form in the expression, whereas the matrix form is applied to the original NMF (7). Therefore, with the definition of l_2-norm, we easily obtain the following equality:

$$\sum_{i=1}^{N} \|(\mathbf{V}_f(i,:)\|^2 \|(\mathbf{V}(i,:)\|^2 = \sum_{i=1}^{N} \Big((\mathbf{V}_f(i,:)\mathbf{V}_f(i,:)^T)(\mathbf{V}(i,:)\mathbf{V}(i,:)^T) \Big) \quad (16)$$

where $()^T$ represent the transpose operation. Meanwhile, suppose we have:

$$\mathbf{A} = \mathbf{V}_f \mathbf{V}_f^T \quad (17)$$

$$\mathbf{B} = \mathbf{V}\mathbf{V}^T \quad (18)$$

then we have $\mathbf{A}_{ii} = (\mathbf{V}_f(i,:)\mathbf{V}_f(i,:)^T)$ and $\mathbf{B}_{ii} = (\mathbf{V}(i,:)\mathbf{V}(i,:)^T)$. Therefore, the term (16) could be rewritten as follows:

$$\begin{aligned} \sum_{i=1}^{N} \|(\mathbf{V}_f(i,:)\|^2 \|(\mathbf{V}(i,:)\|^2 &= \sum_{i=1}^{N} \mathbf{A}_{ii}\mathbf{B}_{ii} \\ &= tr(\mathbf{A} \odot \mathbf{B}) \\ &= tr\Big((\mathbf{V}_f \mathbf{V}_f^T) \odot (\mathbf{V}\mathbf{V}^T) \Big) \end{aligned} \quad (19)$$

where $\odot$ is the Hadamard (elementwise) product and $tr()$ is the trace of matrix. With similar implementation on the term $\sum_{i=1}^{N}(\langle \mathbf{V}_f(i,:), \mathbf{V}(i,:) \rangle)^2)$ in equation (15), we have

$$\sum_{i=1}^{N} (\langle \mathbf{V}_f(i,:), \mathbf{V}(i,:) \rangle)^2 = tr\Big((\mathbf{V}_f \mathbf{V}^T) \odot (\mathbf{V}\mathbf{V}_f^T) \Big) \quad (20)$$

Based on the equalities (19) and (20), we obtain an equivalent form of term (15) as follows:

$$\mathbf{S}(\mathbf{V}_{f(\mathbf{W},\mathbf{H})}) = tr((\mathbf{V}_f \mathbf{V}_f^T) \odot (\mathbf{V}\mathbf{V}^T)) - tr((\mathbf{V}_f \mathbf{V}^T) \odot (\mathbf{V}_f \mathbf{V}^T)) \quad (21)$$

This is, perhaps, a more useful result compared with the original form (10) and (15) as it not only represents the parallelism of all the pixels in HSI, but also benefits the latter calculation of gradient.

Note that the term $\mathbf{F}(\mathbf{W},\mathbf{H})$ in (7) and $\mathbf{S}(\mathbf{V}_{f(\mathbf{W},\mathbf{H})})$ in (21) share some similar characteristics: First, both are theoretically non-negative because $\mathbf{W}$ and $\mathbf{H}$ are non-negative. Moreover, they would be positive in practical applications, because the spectra of the fused HSI would not be completely parallel to those of the original HSI. Also the obtained $\mathbf{W}$ and $\mathbf{H}$ cannot completely reconstruct the original data $\mathbf{V}$ since the introduction of high-frequency information in PI. Second, both the terms should be minimized to obtain the best $\mathbf{W}$ and $\mathbf{H}$ to reconstruct the data $\mathbf{V}$ and preserve the spectral information. Meanwhile, they all have the reference value 0. Third, both terms are coupled for they contain the same $\mathbf{W}$ and $\mathbf{H}$ thus implying that the two terms should be associated instead of individually minimized. Finally, it is also worth mentioning that, $\mathbf{S}(\mathbf{V}_{f(\mathbf{W},\mathbf{H})})$ is proportional to fourth power of matrix elements whereas the term $\mathbf{F}(\mathbf{W},\mathbf{H})$ in (7) is proportional to squares power of matrix elements, thus implying the different level of numerical value between optimization term (7) and (21). Therefore, if addition is adopted, then the carefully tuning of parameters, a quite difficult problem for each experiment, is inevitable.

Based on the previous discussion, we multiply the spectral constraint function (21) and the original NMF model (7), then obtain the fusion model MS-NMF:

$$\begin{aligned} &min \quad \mathbf{G}(\mathbf{W},\mathbf{H}) = \mathbf{F}(\mathbf{W},\mathbf{H}) \times \mathbf{S}(\mathbf{V}_{f(\mathbf{W},\mathbf{H})}) \\ &s.t. \quad \mathbf{W} \geq 0, \mathbf{H} \geq 0. \end{aligned} \tag{22}$$

where $\mathbf{F}(\mathbf{W},\mathbf{H}) = \frac{1}{2}\left\|\mathbf{V}-\mathbf{W}\mathbf{H}\right\|^2$ and $\mathbf{S}(\mathbf{V}_{f(\mathbf{W},\mathbf{H})})$ is defined in (21).

Finally, we obtain the fused data:

$$\mathbf{V}_f = (\mathbf{W}+\mathbf{P}_h)/2 \times \mathbf{H} \tag{23}$$

where $\mathbf{P}_h$ is replication of high-frequency information of original PI, and it has the same size of $\mathbf{W}$. In this model, we see that the spatial quality of the HSI is enhanced by the PI. Meanwhile, the spectral quality is preserved by using the proposed spectral constraint $\mathbf{S}(\mathbf{V}_{f(\mathbf{W},\mathbf{H})})$. Next, we discuss how to solve this optimization problem.

3.4 Numerical Solution for the Fusion Model

In order to solve the previous optimization problem, we use the gradient descent method. We first obtain the partial derivatives of $\mathbf{G}(\mathbf{W},\mathbf{H})$ in model (22):

$$\begin{aligned}\nabla_{\mathbf{W}}\mathbf{G}(\mathbf{W},\mathbf{H}) = &\frac{1}{2}\mathbf{F}(\mathbf{W},\mathbf{H})(diag(\mathbf{V}\mathbf{V}^T)\mathbf{W}\mathbf{H}\mathbf{H}^T + diag(\mathbf{V}\mathbf{V}^T)\mathbf{P}\mathbf{H}\mathbf{H}^T \\ &-diag(\mathbf{W}\mathbf{H}\mathbf{V}^T)\mathbf{V}\mathbf{H}^T - diag(\mathbf{P}\mathbf{H}\mathbf{V}^T)\mathbf{V}\mathbf{H}^T) \\ &+(\mathbf{W}\mathbf{H}-\mathbf{V})\mathbf{H}^T\mathbf{S}(\mathbf{V}_{f(\mathbf{W},\mathbf{H})}) \qquad (24)\\ \nabla_{\mathbf{H}}\mathbf{G}(\mathbf{W},\mathbf{H}) = &\mathbf{F}(\mathbf{W},\mathbf{H})(\mathbf{W}_0^T diag(\mathbf{V}\mathbf{V}^T)\mathbf{W}_0\mathbf{H} \\ &-\mathbf{W}_0^T diag(\mathbf{W}_0\mathbf{H}\mathbf{V}^T)\mathbf{V}) \\ &+\mathbf{W}^T(\mathbf{W}\mathbf{H}-\mathbf{V})\mathbf{S}(\mathbf{V}_{f(\mathbf{W},\mathbf{H})}) \qquad (25)\end{aligned}$$

where $\mathbf{W}_0 = (\mathbf{W} + \mathbf{P}_h)/2$ and $diag(*)$ is diagonal matrix of the matrix $(*)$. Using the steepest descent method [29], we have the following whole algorithm for MS-NMF in Algorithm 1:

Algorithm 1: MS-NMF approximation

---

1. Initialize matrices $\mathbf{W} \geq \mathbf{0}, \mathbf{H} \geq \mathbf{0}$ with vertex component analysis (VCA) method [28]. Set learning rate $\alpha = 10^{-6}$, $\mathbf{G_{old}} = 0$.
2. Calculate the partial derivatives $\nabla_{\mathbf{W}}\mathbf{G}(\mathbf{W},\mathbf{H})$ and $\nabla_{\mathbf{H}}\mathbf{G}(\mathbf{W},\mathbf{H})$ in (24) and (25), respectively. Begin iteration:

a) **While**

$$|\frac{\mathbf{G}_{old} - \mathbf{G}(\mathbf{W},\mathbf{H})}{\mathbf{G}(\mathbf{W},\mathbf{H})}| > tol, \;\; tol \in \mathbb{R}^+$$

b) Update $\mathbf{W}$ and $\mathbf{H}$ by the following step:

$$\begin{aligned}\mathbf{G}_{old} &= \mathbf{G}(\mathbf{W},\mathbf{H}) \\ \mathbf{W}^{k+1} &= max\{0, \mathbf{W}^k - \alpha\nabla_{\mathbf{W}}\mathbf{G}(\mathbf{W},\mathbf{H})\} \\ \mathbf{H}^{k+1} &= max\{0, \mathbf{H}^k - \alpha\nabla_{\mathbf{H}}\mathbf{G}(\mathbf{W},\mathbf{H})\}\end{aligned}$$

c) **End While**

3. Obtain $\mathbf{W}, \mathbf{H}$.
4. Return the fused data by $\mathbf{V}_f = (\mathbf{W} + \mathbf{P})/2 * \mathbf{H}$.

---

where α is the learning rate. $max\{0, \mathbf{W}^k - \alpha\nabla_{\mathbf{W}}\mathbf{G}(\mathbf{W},\mathbf{H})\}$ and $max\{0, \mathbf{H}^k - \alpha\nabla_{\mathbf{H}}\mathbf{G}(\mathbf{W},\mathbf{H})\}$ ensure that both $\mathbf{W}$ and $\mathbf{H}$ are non-negative. Note that in the algorithm, VCA method is applied to initialize the endmemeber matrix $\mathbf{H}$. To obtain the abundance matrix $\mathbf{W}$, least square method (LSM) [39,5] and fully constrained least squares (FCLS) [18] are employed, thus forming MS-NMF with LSM and MS-NMF with FCLS. In the experiments, comparisons between them are implemented.

4 Numerical Experiments

4.1 Quality Indices for Assessing Image Fusion

In order to quantitatively evaluate the performance of different fusion methods, a number of indices are required to be computed and assess the correlations between the fused images, the original images and the reference images. In the paper, the following typical metrics will be applied to assess the different fusion methods:

1. Average Gradient (AG). This index is used to characterize the details of image. For an image without noise, the larger AG is, the image we obtained is better in its spatial information.

2. Entropy (E). The entropy [9,36] of an image reflects the average information content of an image. The larger value it is, the more information the image contains.

3. Correlation Coefficient (CC) [45]. CC evaluates the correlation degree of the fused image and the original images band by band. Here we use it to evaluate the correlation between the fused and original HSI.

4. Spectral Angle Mapper (SAM). The definition is shown as in (9). Obviously, it is an important index in describing the performance of spectral preservation. In our experiments, we calculate the SAM in all pixels, and use their mean value as our final result.

5. Spectral Information Divergence (SID). SID is used to estimate the similarity of pixel spectra between and after fusion [6], and it makes use of the relative entropy to account for the spectral information, so it is effective in characterizing the spectral features.

6. Root Mean Square Error (RMSE). It describe the difference between the original and fused image for the pixels in each image with reference value 0.

7. Erreur Relative Globale Adimensionnelle de *Synthèse* (ERGAS) [4,46] is proposed to summarizes the global errors in all the bands with reference value 0.

Among the seven metrics, AG and E are used to evaluate the properties of the fused HSI. CC, SAM and SID are used to evaluate the correlations between the fused HSI and the original HSI (interpolation version), whereas RMSE and ERGAS are used to evaluate the correlations between the fused

HSI and the reference HSI [4].

4.2 Fusion Results of Simulated Images

To assess the quality of different fusion methods, two properties are checked in the simulated fusion. One is the synthesis of both spatial and spectral information, which requires the fused image being clear in spatial quality. The other is the consistency property, which means that the fused image should be as identical as possible to the reference image or the original image [41].

In the simulation experiment, we use the HSI free from `https://engineering.purdue.edu/~biehl/MultiSpec/hyperspectral.html`. It is collected from the Hyperspectral Digital Imagery Collection Experiment (HYDICE) sensor with 210 spectral channels. It has spectral resolution of 10 nm that acquired from 0.4 μm to 2.4 μm and the size is 307 $\times$ 307 pixels. After low-SNR(signal to noise ratio) bands are removed, only 162 bands remain. To simulate PI with high spatial resolution, we first pick the bands of the original data with the spectral channel 0.5$-$0.76 μm, the wavelength that PI usually covers. Therefore, we calculate the mean of images within the channel, treat it as the original PI. While simulating the HSI, considering the memory of the computer, we need to further remove some bands. Therefore, 62 bands are randomly removed in the experiments. Note that, these bands are randomly removed instead of picking a special wavelength range, thus demonstrating the efficacy of the proposed method on HSI with a wide wavelength range. Then, we spatially degrade each band of the HSI to 77 $\times$77 pixels. Finally, the degraded version is upsampled to 307 $\times$ 307 pixels by bilinear interpolation. We use it as the original HSI for fusion. Thus, the original two different source images are registered by default and shown in Fig. 3.

The proposed method is implemented to make a comparative analysis with some commonly used fusion methods, namely, DWT [38], Ehlers [14], HPF [47], GS, AWLP [3], SPNMF [50], MAP [17]. As discussed in Algorithm 1, two different methods, including LSM and FCLS are used to obtain the abundance matrix $\mathbf{W}$ in the initialization of MS-NMF. Comparison between them will also be implemented in the experiment.

Critical parameters for the different methods are as follows: For DWT and AWLP method, two levels of decompositions are used. For Ehlers method, hanning filter is used, and the cut-off frequency of low pass filter and high pass filter are respectively with order n = 32 and n = 16, as the paper [14] does. The size of window for HPF is 5 $\times$ 5 pixels. The software environment for visualizing images (ENVI) is used to implement the fusion process with the method GS. For SPNMF, the weighted coefficient α is set 0.4 and the

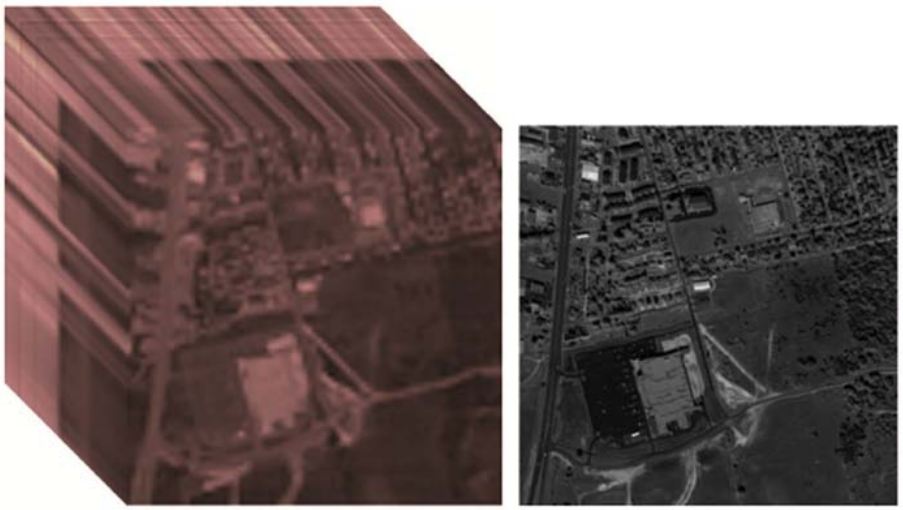

Fig. 3. Original HSI and PI in experiment 1. (a) The original HSI. (b) The original PI.

constant weight β is set 10^{-3}. For the proposed method, learning rate is set 10^{-6}, and the number of endmember number is 5. It is also worth mentioning that, accurate estimating the number of endmembers in HSI is quite difficult, although some estimation methods have been proposed currently [7,13]. In our experiment, virtual dimensionality is used to determine the endmember number like in the paper [19].

Fig. 4(a) shows the degraded HSI with size of 77 $\times$ 77 pixels. Fig. 4(b) shows the interpolated HSI with size of 307 $\times$ 307 pixels, and it is the source image that we use in the experiment. Fig. 4(c) shows the reference image. Fig. 4(d)-(l) are the fused results obtained by the methods DWT, Ehlers, HPF, GS, AWLP, SPNMF, MAP, MS-NMF with LSM and MS-NMF with FCLS, respectively.

By visually comparing the fused images with the original source image and the reference image, we see that the fused HSIs are all sharpened to some extent compared with the original HSI in Fig. 4(b). However, the fused images in Fig. 4 (d),(e) and (i) via the methods DWT, Ehlers and SPNMF are blurred in some degree. On the other hand, by comparing the color of fused images in Fig. 4(f) and (g) with that in Fig. 4(b), obviously, the fused image has obviously higher luminance than the original image. In Fig. 4(e), the color of the building also changes compared with in result Fig. 4(b) which implies that the fused images obtained by the methods Ehlers, HPF, and GS have color distortion. From Fig. 4(h) and (j), it seems that the methods AWLP and MAP obtain the similar fused results. So the similar results in Fig. 4(k) and (l), Although Fig. 4(l) seems to have more bright color because of slight color distortion, it has clearer details in the roof compared with other results.

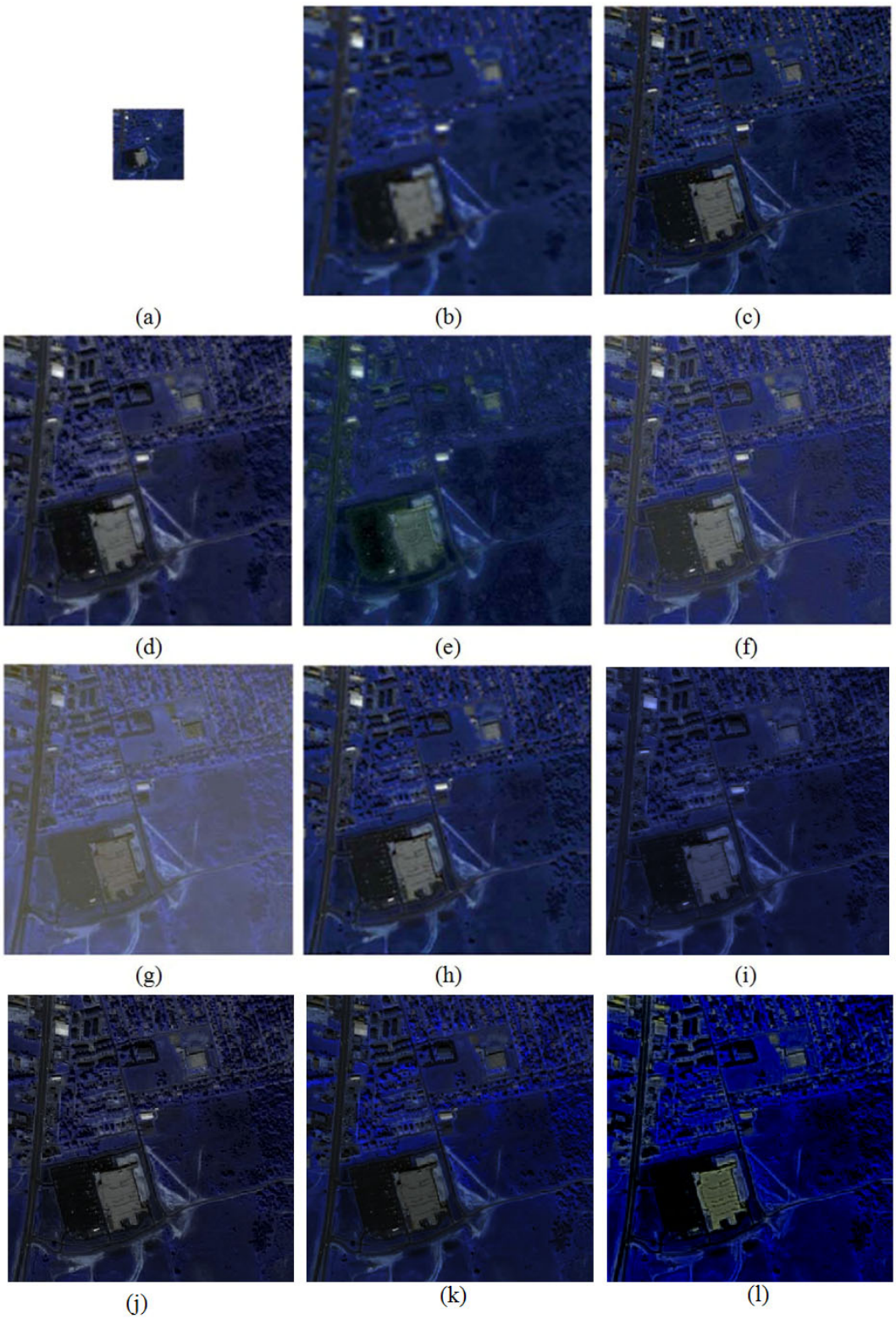

Fig. 4. Original HSI and fused images in simulating experiment. (a) The degraded original HSI with 77 × 77 pixels. (b) The interpolated HSI with size of 307 × 307 pixels. (c) The reference HSI. (d)-(l) are the fused results with the other methods DWT, Ehlers, HPF, GS, AWLP, SPNMF, MAP, MS-NMF with LSM and MS-NMF with FCLS. All the images are shown in false color with bands 10, 30, 60.

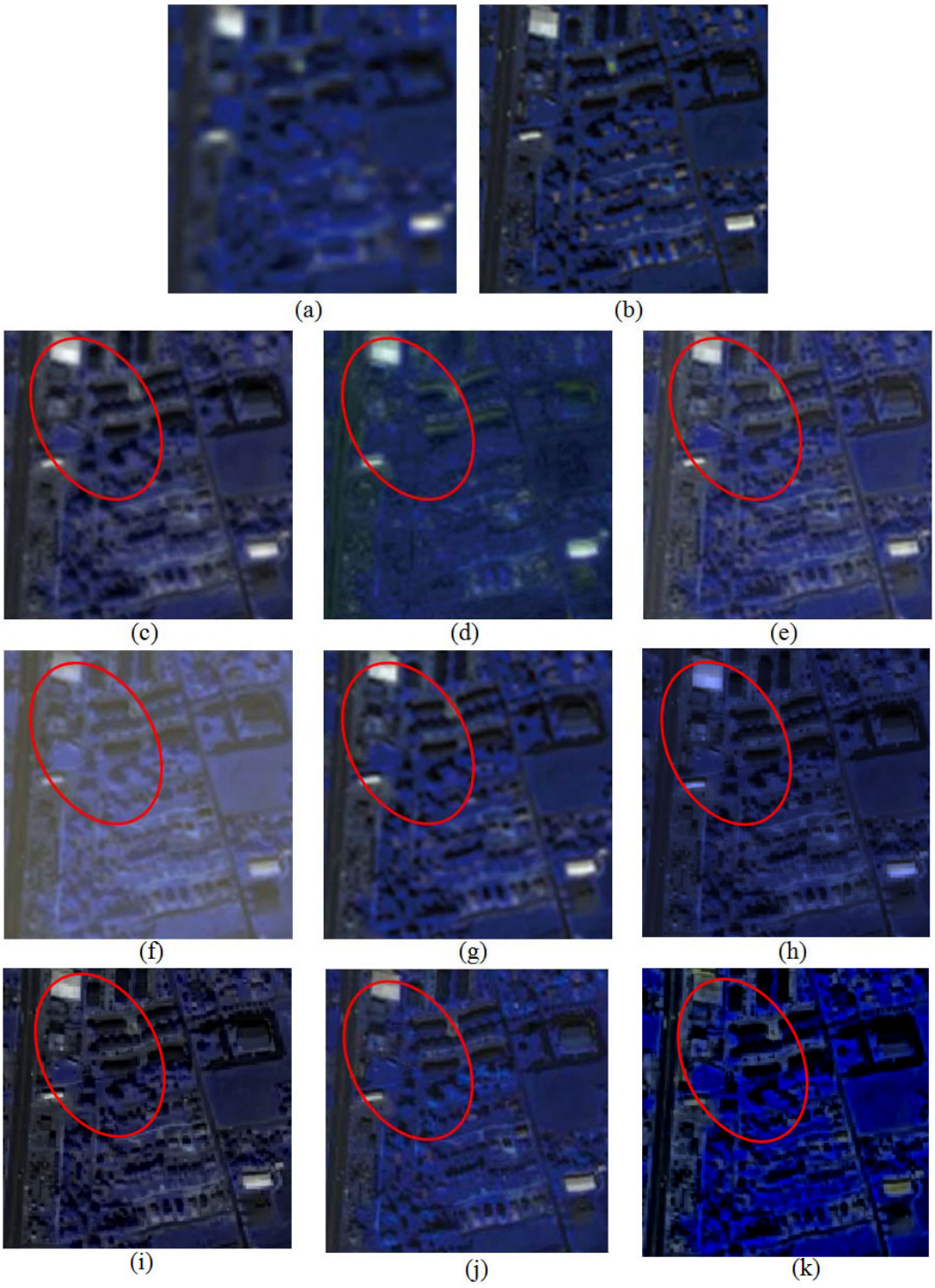

Fig. 5. Subscenes of the original HSI, reference HSI and fused HSIs by different methods (double zoomed). (a) - (b) The original HSI and the reference HSI. (c)-(k) The subscenes of fused HSIs by methods DWT, Ehlers, HPF, GS, AWLP, SPNMF, MAP, MS-NMF with LSM and MS-NMF with FCLS, respectively. All the images are shown in false color with bands 10, 30, 60.

To clearly see the details, we illustrate the subscenes of the original, reference and fused HSI with double zooming in Fig. 5. Compared with Fig. 5(j), Fig. 5(k) have more color distortion for the roofs become gray whereas they are white in the original and reference HSI (Fig. 5(a) and (b), respectively). Compared with the Fig. 5(c), (d), (h) and (i), Fig. 5(j) and (k) also have clearer edges. Meanwhile, compared with the Fig. 5(e) and (f), Fig. 5(j) obtains the result which is closest to the original image. Therefore, the proposed MS-NMF method provides high-quality spatial details while preserving color well.

Table 1
Evaluation results of the simulated experiment

	AG	E	CC	SAM	SID	RMSE	ERGAS
DWT	0.0214	6.4924	0.8532	3.7138	0.0762	1.0911	12.1884
Ehlers	0.0213	6.6939	***0.9359***	6.7069	0.0146	1.4255	8.8062
HPF	0.0276	6.3402	0.8854	5.4977	0.0624	2.4122	19.8292
GS	0.0275	6.5360	0.8882	11.0082	0.2217	4.8774	46.0235
AWLP	0.0268	6.4793	0.8854	3.2416	0.0323	1.3250	10.6380
SPNMF	0.0191	6.3947	0.9225	5.2058	0.0127	0.8680	6.5192
MAP	0.0288	6.4898	0.8040	12.1253	0.1311	1.8193	19.3487
MS-NMF with LSM	0.0295	6.5361	0.8863	***2.6877***	***0.0025***	***0.5918***	***3.7912***
MS-NMF with FCLS	***0.0462***	***7.1589***	0.7736	4.7009	0.0111	2.2529	13.7435

The indices illustrated in Table 1 could help us quantitatively evaluate the performance of different fusion methods. The bold italic font is the best one in the same column. Since the reference HSI could be obtained in the simulated experiments, the indices RMSE and ERGAS are calculated in the experiment. From Table 1, we see that, the two indices RMSE and ERGAS obtained by the proposed MS-NMF with LSM method behaves best among all the methods, which implies that, the proposed method obtains the fused data which is the closest to the reference image. As mentioned, AG and E are indices representing the clarity and the information of an image, respectively. According to Table 1, the fused HSI by the proposed MS-NMF with FCLS method have the best AG and E. It implies that, the proposed fusion method enhances the spatial quality of HSI effectively. Indices SAM and SID all describe the spectral correlations of the fused HSIs and the original HSIs. In the proposed method, the spectral information of the original HSI is preserved well (indices SAM and SID in Table 1 confirm this) since the spectral constraint is introduced. Therefore, though the index CC is not the best in the proposed method, the indices SAM and SID confirm the preservation of the spectral information.

4.3 Fusion Results of Real Images

In the experiment on the real image, free HSI is obtained from `https://engineering.purdue.edu/~biehl/MultiSpec/hyperspectral.html`. Subscene of the Washington DC is illustrated in Fig. 6(a), which contains 150 × 250 pixels. Only 64 bands remain after low-SNR bands are removed. Meanwhile, by using the free software Universal Maps Downloader (a simple yet effective tool) from `http://www.softonpc.com/umd/`, PI (as shown in Fig. 6(b)) could be obtained from the Google map, and its spatial resolution is twice of the HSI. They are registered manually before the fusion.

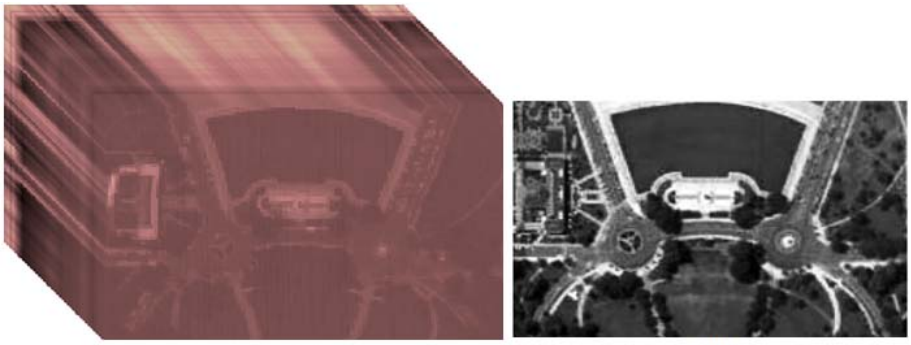

Fig. 6. Original HSI and PI in experiment 2. (a) The original HSI. (b) The original PI.

Fig. 7 shows the original and fused HSIs obtained with different methods. Fig. 7(a) is the original HSI. (b) - (d) are the fused results with the methods DWT, Ehlers, HPF, GS, AWLP, SPNMF, MAP, MS-NMF with LSM and MS-NMF with FCLS, respectively. All the images are also illustrated in false color with bands 10, 30, 60. The indices in Table 2 also show the evaluation results in the experiment 2. The bold italic font is the best one in the same column. It is worth mentioning that the calculations of indices RMSE and ERGAS require reference HSI, which we can not obtain in real world. Therefore, table 2 lacks those two indices. On the other hand, indices CC, SAM and SID are used to assess the correlations between the fused HSI and the original HSI, therefore, in the experiment with real data, the above three indices are calculated with the fused and original HSI, as the paper [4] does.

From Fig. 7(b) and (d), we see that the methods DWT and HPF distort the color of the original HSI in Fig. 7(a). The roads in Fig. 7(f) are also distorted. It implies that, the methods DWT, HPF and AWLP possibly result in spectral distortion in some degree if they are used in HSI fusion. Meanwhile, from Fig. 7(i) and (j), we see that, both MS-NMF with LSM and FCLS obtain fused HSIs with good spatial quality, so as the fusion results in Fig. 7(e), (g) and (h), which obtained with methods GS, SPNMF and MAP, respectively. It is difficult for evaluating those results visually, therefore, the indices in table

2 are helpful for quantitative evaluation. From the indices CC, SAM and SID in Table 2, we see that the proposed MS-NMF with FCLS behaves better in spectral preservation implying that the proposed method preserves the spectral information effectively. Meanwhile, AG and E of the proposed method are close to the best (obtained by the method DWT and MAP, respectively). Therefore, the proposed method performs better in the fusion of HSI and PI than the conventional methods in experiments on both the simulated and the real world data.

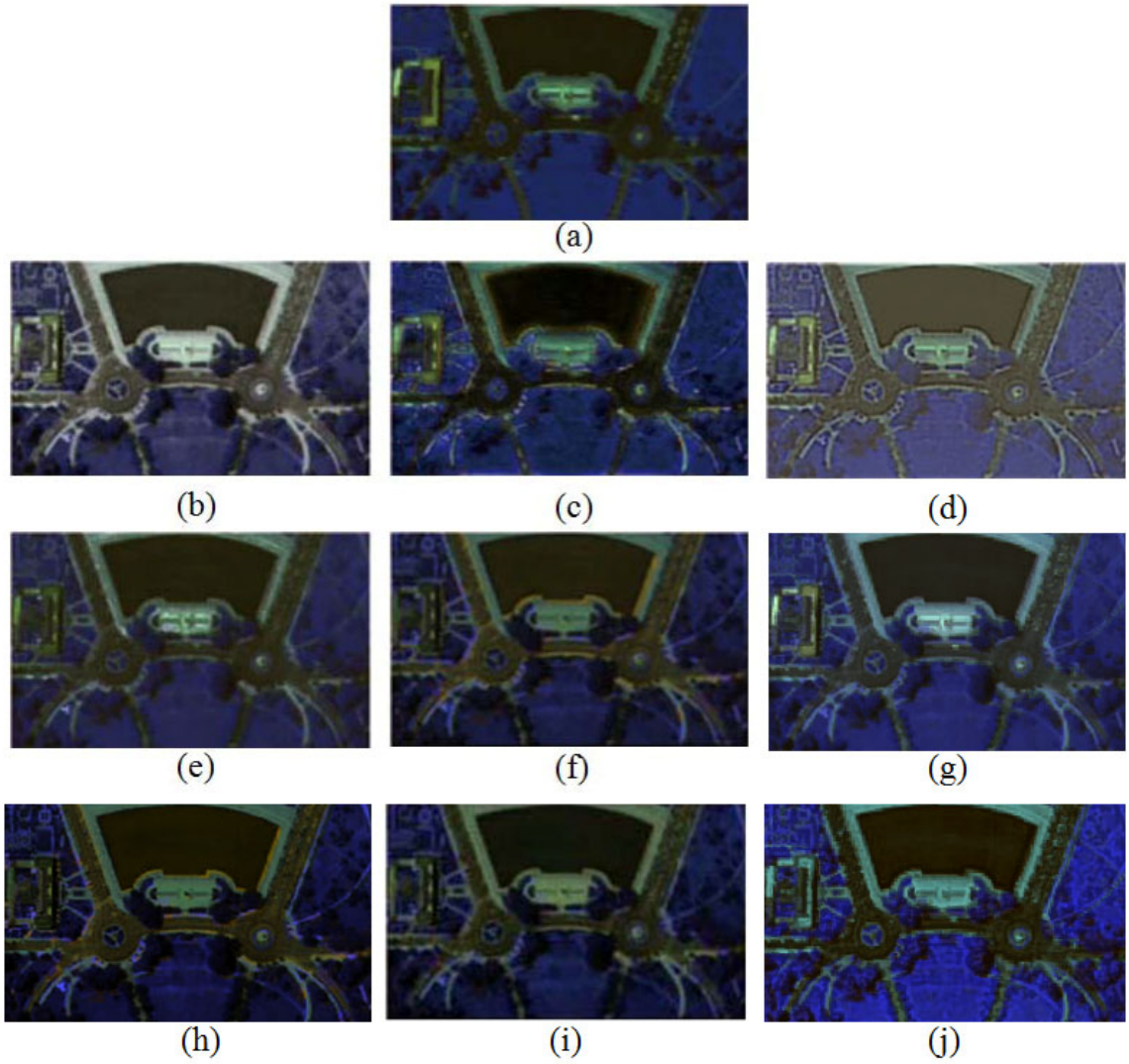

Fig. 7. Original HSI and fused images in experiment 2. (a) The original HSI with 150×250 pixels. (b)-(j) are the fused results with the other methods DWT, Ehlers, HPF, GS, AWLP, SPNMF, MAP, MS-NMF with LSM and MS-NMF with FCLS. All the images are shown in false color with bands 10, 30, 60.

Table 2
Evaluation results of the experiment 2

	AG	E	CC	SAM	SID
DWT	***0.0418***	6.8245	0.6514	15.9504	0.1458
Ehlers	0.0299	6.5982	0.7634	12.7090	0.0543
HPF	0.0358	6.3402	0.7117	20.2816	0.1036
GS	0.0203	6.5360	0.7947	30.6946	0.0870
AWLP	0.0326	6.9484	0.5286	9.5986	0.0554
SPNMF	0.0198	6.4293	0.8459	4.1366	0.0067
MAP	0.0370	***7.0180***	0.6097	3.3216	0.0319
MS-NMF with LSM	0.0244	5.8745	0.8836	3.4732	0.0048
MS-NMF with FCLS	0.0329	6.3614	***0.9002***	***3.2097***	***0.0046***

5 Conclusions

In the paper, a hyperpsectral image fusion model MS-NMF is proposed. It is based on the multiplication of original NMF and the proposed spectral constraint function. In the model, HSI is first factorized into the abundance matrix and endmember matrix. Then the abundance matrix is enhanced with PI. Meanwhile, to preserve the spectral information of the original HSI, a simplified spectral constraint function is proposed and specifically utilized in the model. Therefore, compared with the conventional methods, we see that the proposed method is designed according to the feature of HSI. With exploiting different initializing methods LSM and FCLS, MS-NMF has two different forms. In the experiments with synthetical and the real world data, visual analysis and quantitative assessment are implemented. From the results, we see that, both forms of the proposed methods have obvious advantages in simultaneously preserving the spatial and spectral information. Specifically, MS-NMF with FCLS behaves better in spatial information in both simulated and real data, while MS-NMF with LSM seems to behave better in spectral preservation in simulated data. It is also worth mentioning that, besides the proposed enhancement process and applied optimization algorithm, more effective approaches would benefit the fusion result, implying the wide extendibility of MS-NMF.

References

[1] M. L. S. Aguena, N. Mascarenhas, Multispectral image data fusion using projections onto convex sets techniques, in: Proceedings of Computer Graphics and Image Processing (2002) pp. 76-82.

[2] C. Ballester, V. Caselles, L. Igual, J. Verdera, A variational model for P+XS image fusion, International Journal of Computer Vision 69(1)(2006) 43-58.

[3] P. Blanc, T. Blu, T. Ranchin, L. Wald, R. Aloisi, Using iterated rational filter banks within the ARSIS concept for producing 10m Landsat multi-spectral images, International Journal of Remote Sensing 19(12)(1998) 2331-2343.

[4] M. Cetin, N. Musaoglu, Merging hyperspectral and panchromatic image data: qualitative and quantitative analysis, International Journal of Remote Sensing 30(7)(2009) 1779-1804.

[5] C.-I. Chang, X. Zhao, M. L. G. Althouse, J.-J. Pan, Least squares subspace projection approach to mixed pixel classification in hyperspectral images, IEEE Trans. Geosci. Remote Sensing 36(3)(1998) 898-912.

[6] Chein-I. Chang, An information theoretic-based approach to spectral variability, similarity and discriminability for hyperspectral image analysis, IEEE Transactions on Information Theory 46(5)(2000) 1927-1932.

[7] Chein-I. Chang, Q. Du, Estimation of number of spectrally distinct signal sources in hyperspectral imagery, IEEE Trans. Geosci. Remote Sensing 42(3)(2004) 608-619.

[8] P. S. Chavez, J. A. Bowell, Comparison of the spectral information content of Landsat thematic mapper and SPOT for three different sites in the phoenix, Arizona region, Photogrammetric Engineering and Remote Sensing 54(12)(1988) 1699-1708.

[9] Y. Chen, Z. Y. Xue, R. S. Blum, Theoretical analysis of an information-based quality measure for image fusion, Information Fusion 9(2)(2008) 161-175.

[10] M. Choi, A new intensity-hue-saturation fusion approach to image fusion with a tradeoff parameter, IEEE Transaction of Geoscience and Remote Sensing 44(6)(2006) 1672-1682.

[11] T. M. Cover, J. A. Thomas, Elements of information theory, Wiley-Interscience (2006).

[12] M. Deshmukh, U. Bhosale, Image fusion and image quality assessment of fused images, International Journal of Image Processing 4(5)(2010) 484-508.

[13] J. M. B. Dias, J. M. P. Nascimento, Hyperspectral subspace identification, IEEE Transactions on Geoscience and Remote Sensing 46(8)(2008) 2435-2445.

[14] M. Ehlers, Spectral characteristics preserving image fusion based on fourier domain filtering, in: Proceedings of SPIE-Remote Sensing Environmental Monitoring. GIS Applications, and Geology. IV, Maspalomas, Gran Canaria, Spain (2004) pp. 1-13.

[15] M. T. Eismann, R. C. Hardie, Hyperspectral resolution enhancement using high-resolution multispectral imagery with arbitrary response functions, IEEE Transactions on Geoscience and Remote Sensing 43(3)(2005) 455-465.

[16] A. F. H. Goetz, G. Vane, J. E. Solomon, B. N. Rock, Imaging spectrometry for earth remote sensing, Science 228(1985) 1147-1153.

[17] R. C. Hardie, M. T. Eismann, G. L. Wilson, MAP estimation for hyperspectral image resolution enhancement using an auxiliary sensor, IEEE Transaction on Image Processing 13(9)(2004) 1174-1184.

[18] D. C. Heinz, C.-I. Chang, Fully constrained least squares linear spectral mixture analysis method for material quantification in hyperspectral imagery, IEEE Transactions on Geoscience and Remote Sensing 39(3)(2001) 529-545.

[19] S. Jia, Y. T. Qian, Constrained nonnegative matrix factorization for hyperspectral unmixing, IEEE Transactions on Geoscience and Remote Sensing 47(1)(2009) 161-173.

[20] M. S. Karoui, Y. Deville, S. Hosseini, A. Ouamri, Blind spatial unmixing of multispectral images: new methods combining sparse component analysis, clustering and non-negativity constraints, Pattern Recognition 45(12)(2012) 4263-4278.

[21] Yonghyun Kim, Changno Lee, Dongyeob Han, Yongil Kim, Younsoo Kim, Improved additive-wavelet image fusion, IEEE geoscience and remote sensing letters 8(2)(2011) 263-267.

[22] R. L. King, J. Wang, A wavelet based algorithm for pan sharpening Landsat 7 imagery, in: Proceedings of International Geoscience and Remote Sensing Symposium (IGARSS 2001), 9-13 July 2001, Sydney, Australia (2001) pp. 849-851.

[23] U. Kumar, C. Mukhopadhyay, T. V. Ramachandra, Pixel based fusion using IKONOS imagery, International Journal of Recent Trends in Engineering 1(1)(2009) 173-177.

[24] D. Landgrebe, Hyperspectral image data analysis, IEEE Signal Processing Magazine 19(1)(2002) 17-28.

[25] H. Lee, A. Cichocki, S. Choi, Kernel non-negative matrix factorization for spectral EEG feature extraction, Neurocomputing 72(2009) 3182-3190.

[26] D. D. Lee, H. S. Seung, Learning the parts of objects by non-negative matrix factorization, Science 401(1999) 788-791.

[27] G. A. Licciardi, M. K. Murtaza, J. Chanussot, A. Montanvert, L. Condat, C. Jutten, Fusion of hyperspectral and panchromatic images using multiresolution analysis and nonlinear PCA band reduction, in: Geoscience and Remote Sensing Symposium (IGARSS), 2011 IEEE International (2011) pp. 1783-1786.

[28] J. M. P. Nascimento, J. M. B. Dias, Vertex component analysis: A fast algorithm to unmix hyperspectral data, IEEE Transactions on Geoscience and Remote Sensing 43(4)(2005) 898-910.

[29] N. Nocedal, S. J. Wright, Numerical Optimization, 2nd ed. Springer (2006).

[30] J. N*úñ*ez, X. Otazu, O. Fors, A. Prades, V. Pal, R. Arbiol, Multiresolution-based image fusion with additive wavelet decomposition, IEEE Transaction on Geoscience and Remote Sensing 37(3)(1999) 1204-1211.

[31] G. Piella, A general framework for multiresolution image fusion: from pixels to regions, Information Fusion 4(4)(2003) 259-280.

[32] C. Pohl, J. L. van Genderen, Multisensor image fusion remote sensing: concepts, methods and applications, International Journal of Remote Sensing 19(5)(1998) 823-854.

[33] P. S. Pradhan, R. L. King, N. H. Younan, D. W. Holcomb, Estimation of the number of decomposition levels for a wavelet-based multiresolution multisensor image fusion, IEEE Transaction on Geoscience and Remote Sensing 44(12)(2006) 1683-1691.

[34] T. Ranchin, L. Wald, Fusion of high spatial and spectral resolution images: the ARSIS concept and its implementation, Photogrammetric Engineering and Remote Sensing 66(1)(2000) 49-61.

[35] T. Ranchin, B. Aiazzi, L. Alparone, S. Baronti, L. Wald, Image fusion - the ARSIS concept and some successful implementation Schemes, ISPRS Journal of Photogrammetry Remote Sensing 58(2003) 4-18.

[36] J. W. Roberts, J. V. Aardt, F. Ahmed, Assessment of image fusion procedures using entropy, image quality, and multispectral classification, Journal of Applied Remote Sensing 2(1)(2008) 1-28.

[37] M. J. Shensa, The discrete wavelet transform: wedding the a trous and mallat algorithms, IEEE Transaction on Signal Processing 40(10)(1992) 2464-2482.

[38] V. K. Shettigara, A generalized component substitution technique for spatial enhancement of multispectral images using a higher resolution data set, Photogrammetric Engineering and Remote Sensing 58(5)(1992) 561-567.

[39] Y. E. Shimabukuro, J. A. Smith, The least-squares mixing models to generate fraction images derived from remote sensing multispectral Data, IEEE Trans. Geosci. Remote Sensing 29(1)(1991) 16-20.

[40] Z. W. Shi, Z. Y. An, Z. G. Jiang, Hyperspectral image fusion by the similarity measure based variational method, Optical Engineering 50(7)(2011): 077006.

[41] C. Thomas, T. Ranchin, L. Wald, J. Chanussot, Synthesis of multispectral images to high spatial resolution: A critical review of fusion methods based on remote sensing physics, IEEE Transaction on Geoscience and Remote Sensing 46(5)(2008) 1301-1312.

[42] T. M. Tu, S. C. Su, H. C. Shyu, P. S. Huang, A New look at IHS-like image fusion methods, Informaiton Fusion 2(3)(2001) 177-186.

[43] T. M. Tu, P. S. Huang, C.-L. Hung, C.-P. Chang, A fast intensity-hue-saturation fusion technique with spectral adjustment for IKONOS imagery, IEEE Geoscience and Remote Sensing Letters 1(4)(2004) 309-12.

[44] G. Vane, A. F. H. Goetz, Terrestrial imaging spectrometry: current status, future trends, Remote Sensing of Environment 44(2)(1993) 109-127.

[45] V. Vijayaraj, C. G. O. Hara, N. H. Younan, Quality analysis of pansharpened images, in: Proceedings of IEEE International Geoscience and Remote Sensing Symposium, Mississippi State Univ., Starkville. 1(2004) pp. 85-88.

[46] L. Wald, Data Fusion Definitions and Architectures, Fusion of images of different spatial resolutions, Paris: Les Presses de l'Ecole des Mines 2002.

[47] Zhijun Wang, Djemel Ziou, Costas Armenakis, Deren Li, Qingquan Li, A comparative analysis of image fusion methods, IEEE Transaction on Geoscience and Remote Sensing 43(6)(2005) 1391-1402.

[48] N. Yokoya, T. Yairi, A. Iwasaki, Coupled non-negative matrix factorization unmixing for hyperspectral and multispectral data fusion, IEEE Transactions on Geoscience and Remote Sensing 50(2)(2012) 528-37.

[49] N. Yokoya, T. Yairi, A. Iwasaki, Hyperspectral, multispectral, and panchromatic data fusion based on coupled non-negative matrix factorization, in: Proceedings of the 2011 IEEE Workshop on Hyperspectral Image and Signal Processing: Evolution in Remote Sensing (2011) pp. 1-4.

[50] Z. Zhang, Z. W. Shi, Nonnegative matrix factorization-based hyperspectral and panchromatic image fusion, Neural Compt. & Applic, (2012) DOI: 10.1007/s00521-012-1014-2.

[51] Z. Zhang, Z. W. Shi, Z. Y. An, Hyperspectral and panchromatic image fusion using unmixing-based constrained nonnegative matrix factorization, Optik-International Journal for Light and Electron Optics 124(13)(2013) 1601-1608.